Arabian Journal of Chemistry (2023) **16**, 105113

King Saud University

Arabian Journal of Chemistry

www.ksu.edu.sa
www.sciencedirect.com

ORIGINAL ARTICLE

Exploring the potential anti-inflammatory effect of biosynthesized gold nanoparticles using *Isodon excisus* leaf tissue in human keratinocytes

Sanjeevram Dhandapani [a], Rongbo Wang [a], Ki cheol Hwang [b], Hoon Kim [c,*], Yeon-Ju Kim [a,*]

[a] *Graduate School of Biotechnology, and College of Life Science, Kyung Hee University, Yongin-si, 17104, Gyeonggi-do, Republic of Korea*
[b] *Rafarophe Co, Venture Research Center, Cheongju, Republic of Korea*
[c] *Department of Food and Nutrition, Chung Ang University, Seodong-daero 4726, Daedeok-myeon, Anseong 17546, Republic of Korea*

Received 23 May 2023; accepted 25 June 2023
Available online 4 July 2023

KEYWORDS

Isodon excisus;
Gold nano-based treatments;
Skin inflammation;
Autophagy;
PI3K/AKT signaling pathway

Abstract The skin plays a crucial role in maintaining hydration, preventing dehydration, and protecting against harmful microorganisms. Skin injury can lead to inflammation and fluid loss, which are detrimental to human health. Nanotechnology has been proposed as a potential solution to prevent skin damage because it can more effectively penetrate the skin barrier and deliver targeted treatments directly to the cells that require them. In this study, we biosynthesized gold nanoparticles (AuNPs) using *Isodon excisus* (Maxim.) Kudo (IE) leaf tissue. The formation of IE gold nanoparticles (IE-AuNPs) was confirmed using various techniques. Furthermore, the cytotoxicity of IE-AuNPs on human keratinocytes (HaCaT cells) was evaluated, and it was found that the IE-AuNPs had no cytotoxic effect on HaCaT cells (50 μg/mL). The ability of IE-AuNPs to penetrate HaCaT cells and reduce skin inflammation was investigated using dark-field microscopy (DFM) and enzyme-linked immunosorbent assay (ELISA). Real-time quantitative reverse transcription-polymerase chain reaction (qRT-PCR) was used to assess inflammatory biomarkers such as IL-6, IL-8, CCL17/TARC, CCL27/CTACK, and CCL5/RANTES. Additionally, western blotting demonstrated that IE-AuNPs exhibited anti-inflammatory effects on the skin by activating autophagy biomarkers and inhibiting the PI3K/AKT signaling pathway at the upstream level. Overall, our findings suggest that IE-AuNPs enhance the anti-inflammatory effect on skin cells and can

* Corresponding authors at: Graduate School of Biotechnology, and College of Life Science, Kyung Hee University, Yongin-si, 17104, Gyeonggi-do, Republic of Korea.
E-mail addresses: hkim81@cau.ac.kr (H. Kim), yeonjukim@khu.ac.kr (Y.-J. Kim).
Peer review under responsibility of King Saud University.

Production and hosting by Elsevier

https://doi.org/10.1016/j.arabjc.2023.105113

be used in the development of nano-based treatments for skin-related diseases.

1. Introduction

Atopic dermatitis (atopic eczema) is a chronic, relapsing, and remitting inflammatory skin disease that affects approximately one in 10 individuals during their lifetime (Kashaf et al., 2023). The pathogenesis of atopic dermatitis involves a complex interplay between immune dysregulation, epidermal gene mutations, and environmental factors, which collectively disrupt the epidermis and result in the development of intensely pruritic skin lesions (Tai et al., 2023). The repetitive act of scratching initiates a self-perpetuating itch-scratch cycle, further exacerbating the condition and significantly impacting the patient's quality of life. While certain treatments, such as crisaborole and dupilumab, have shown effectiveness in managing atopic dermatitis, their high cost currently limits their accessibility to the majority of patients (Shahin et al., 2023). Therefore, there is an urgent demand for the development of new, affordable, and well-tolerated therapeutic interventions for atopic dermatitis. A substantial body of evidence supports the role of keratinocytes as enhancer cells in immune responses associated with atopic dermatitis (Papa et al., 2023). Keratinocytes, which are the most abundant cells in the epidermis, play a critical role in maintaining the barrier function of the skin and protecting it from external factors. In addition to their protective and structural functions, keratinocytes regulate skin inflammation by producing various proinflammatory cytokines, chemokines, and other signaling molecules that activate immune cells, such as macrophages and dendritic cells, which in turn amplify the inflammatory response (Guan et al., 2023). Keratinocytes express cytokine and chemokine receptors that recruit and activate immune cells to combat inflammation. Keratinocytes play a pivotal role in regulating skin inflammation by interacting with immune cells via various receptors. However, keratinocyte dysfunction can lead to chronic inflammation and skin disorders, including psoriasis, atopic dermatitis, and acne (Calabrese et al., 2022). Therefore, it is necessary to identify therapeutic strategies to treat and protect the keratinocytes of the skin with the aim of preventing and treating skin inflammation as well as meet the unmet medical needs of individuals suffering from diverse skin disorders, leading to improved quality of life and overall skin well-being.

Nanobiotechnology focuses on the development of biodegradable nanomaterials, such as biologically active nanoparticles (NPs), and their potential biomedical applications (Kumar et al., 2022). Nanomaterials possess diverse applications in healthcare, medicine, and drug delivery, including in cell imaging, biosensing, photodynamic therapy, and targeted drug delivery for chemotherapy (Abdel-Mageed et al., 2021). Gold nanoparticles (AuNPs) have received considerable attention because of their tunable plasmon resonance surfaces and unique optoelectronic characteristics, making them promising for use in disease detection and drug delivery, skin disease treatment, cosmetic formulations, and various other biomedical applications (Anik et al., 2022; Khan et al., 2022). However, the physical and chemical production of AuNPs is expensive and can cause environmental issues (Hosny et al., 2022; Rani et al., 2023). Therefore, it is essential to develop a more eco-friendly and cost-effective method for their synthesis (Firdhouse & Lalitha, 2022). Plant-mediated synthesis of metallic NPs is an emerging method that has gained attention. The use of plant extracts for the synthesis of nanomaterials is a potentially green technology because aqueous extracts are simple, affordable, stable, and flexible (Roy et al., 2022; Sahu et al., 2022). Plant leaf extracts have been used as reducing and capping agents in NP synthesis (Dhandapani et al., 2021; Irfan et al., 2022). The alkaloids, polyphenols, flavonoids, and terpenoids present in plant extracts enhance metal ion reduction and promote the production of metal NPs (Kerketta & Sahu, 2023). Bioactive phytomolecules absorbed onto the NP surfaces can also enhance their antioxidant, antibacterial, anti-inflammatory, and anticancer properties (Nadaf et al., 2022). Therefore, green synthesis using plant extracts is a promising approach for improving the bioavailability of nanomaterials and has potentially beneficial effects in skin applications.

Isodon excisus (IE) is a plant species belonging to the Lamiaceae family that is widely found in Korea. It has traditionally been used in folk medicine to treat gastrointestinal and detoxification issues. Recent studies have revealed that the leaves of IE contain various biogenic phytomolecules such as alkaloids, flavonoids, tannins, phenolic compounds, saponins, and triterpenoids, which are responsible for the bioactivity of IE (Sobhy et al., 2022). Previous studies have demonstrated the efficacy of these compounds as natural reducing agents (Dhandapani et al., 2023). Nevertheless, further investigation is required to explore the potential medical properties of AuNPs synthesized using IE as a reducing agent. In this study, we employed the unique green synthesis approach of utilizing the IE leaf extract to synthesize AuNPs through a green and sustainable method. To the best of our knowledge, this is the first study to synthesis AuNPs using natural extracts from IE in conjunction with green nanotechnology.

2. Materials and methods

2.1. Extraction and identification of secondary metabolites from IE leaf tissue

Leaf tissue from IE was collected from the northern Gyeonggi region, located adjacent to the demilitarized zone in the Republic of Korea. The plant identification process was carried out by Dr. J. K. Kim, a senior researcher affiliated with the Gyeonggido Business and Science Accelerator, Gyeonggi Biocenter in Suwon, South Korea. A voucher specimen (GB-0006) was meticulously preserved and cataloged within the department for future reference purposes. The obtained leaf tissue was subjected to air-drying, and the resulting dried material was extracted with 70% ethanol (5 L) over a period of 3 days at temperatures ranging from 20 to 25 °C. The extract was subjected to filtration employing a 20-μm filtering cloth (Hyundai Micro, Anseong, South Korea), followed by concentration using a vacuum evaporator (Buchi Korea Inc., Gwangmyeong, South Korea), and subsequently dried using a lyophilizer (Ilshin Biobase, Daejeon, South Korea). This process yielded a powdered formulation of the 70% ethanolic extract. The main constituents present in the IE were identified using ultra-performance liquid chromatography-tandem mass spectrometry (UPLC-MS/MS; LTQ Orbitrap XL; Thermo Electron, Waltham, MA, USA).

2.2. Synthesis of IE-AuNPs using IE extract

In this experiment, extract from IE was used to facilitate the biosynthesis of AuNPs. The synthesis of IE-AuNPs was conducted at different concentration conditions of $HAuCl_4{\cdot}3H_2O$ (ranging 0.5–2.5 mM) and IE extract (ranging 1.5–3 mg/mL). The reaction temperature (ranging 30–60 °C) and duration (ranging 20–50 min) were also adjusted to generate

optimized IE-AuNPs. The obtained IE-AuNPs were rinsed with distilled water and centrifuged for 20 min at 12,500 rpm. The resulting dried IE-AuNPs sample was placed at 4 °C for further experiments. AuNP generation was detected using a double-beam ultraviolet–visible (UV–Vis) spectrometer (Optizen POP; Mecasys, Daejeon, Korea) at wavelengths ranging 300–800 nm. After optimization, multiple trials were carried out to ensure the accuracy and reliability of the synthesis. Specifically, we performed three independent trials for synthesis.

2.3. Characterization of IE-AuNPs

Transmission electron microscopy (TEM) and energy-dispersive X-ray (EDX) spectroscopy were used to examine the size, shape, and percentage of gold in IE-AuNPs. A sample of the expelled molecule was placed on a TEM grid and images were captured. To detect the development of the particles, X-ray diffraction (XRD), Fourier transform infrared spectroscopy (FT-IR), and selected area electron diffraction (SAED) were used to assess the crystallinity of the NPs. An optical particle analyzer for dynamic light scattering (DLS) was used to identify the NP size and dispersion. Atomic field microscope (AFM) imaging to further investigate the size distribution of the IE-AuNPs. Table S1 lists the characterization techniques used in this study.

2.4. Cell viability of IE-AuNPs on HaCaT cells

The HaCaT (human keratinocyte) cell line was purchased from Cell Line Service (CLS, Eppelheim, Heidelberg, Germany). The HaCaT cells were cultured in Dulbecco's Modified Eagle Medium (DMEM) supplemented with 10% heat-inactivated fetal bovine serum (FBS) and 1% penicillin–streptomycin (PS). The culture was maintained at 37 °C in a humidified incubator with 5% CO_2 and 95% air.

The inhibitory activity of the samples was assessed using a conventional 2,5-diphenyl-2H-tetrazolium bromide (MTT) assay. HaCaT cells were seeded in a 96-well plate at a density of 1×10^5 cells per well and allowed to stabilize. Different concentrations of IE and IE-AuNPs were added to the cells. After 24 h of incubation, the samples were treated with dimethyl sulfoxide (DMSO) for one hour. Subsequently, MTT solution (5 mg/mL) was added, and the formed formazan crystals were allowed to develop. The absorbance of the solution was measured at 570 nm using a microplate reader (SpectraMax® ABS Plus, San Jose, CA, USA).

2.5. Assessment of cellular internalization

HaCaT cells were seeded into culture dishes at a density of 5×10^4 cells per well and allowed to stabilize for 24 h. Following the replacement of the culture medium, the cells were treated with IE-AuNPs at a concentration of 50 μg/mL for either 1 or 3 h. Further, rinse with phosphate-buffered saline (PBS), the cells were fixed using a 4% paraformaldehyde solution obtained from Sigma. Subsequently, the uptake capacity of IE-AuNPs was visualized using a high-resolution enhanced dark-field (EDF) microscopic system provided by Cytoviva, Inc. located in Auburn, USA.

2.6. LIVE/DEAD staining

Cell viability was performed using a LIVE/DEAD staining kit obtained from Invitrogen Biotechnology, Waltham, MA, USA. The staining allowed for differentiation between live cells, which appeared green, and dead cells, which appeared red. After loading the cells into the microfluidic devices, the culture chambers of the microfluidic chip were rinsed with PBS (HyClone) for 1–3 min to clean them. Subsequently, the Live/Dead Cell Imaging Kit was added, and the cells were incubated at 37 °C for 15–30 min. The culture chambers were then examined using a fluorescence microscope.

2.7. ROS and Mito-SOX production

To measure intracellular reactive oxygen species (ROS) release, a cellular ROS/superoxide detection assay kit from Abcam, Cambridge, USA, was employed. HaCaT cells (1×10^5 cells) were seeded in six-well plates and treated with different concentrations of IE and IE-AuNPs for 24 h. Subsequently, 0.4 μL of oxidative stress and superoxide detection reagents were added to the cells. After a 30 min incubation period, fluorescence was quantified using a microscope from Leica Microsystems, Wetzlar, Germany.

2.8. Enzyme-linked immunosorbent (ELISA) analysis

The cells were seeded in 96-well plates at a density of 1×10^5 cells/well. After pretreatment with IE-AuNPs and IE at different concentrations (25 and 50 μg/mL) for 24 h, the cells were exposed to TNF-α/IFN-γ (T + I). The supernatants were collected and analyzed for the presence of pro-inflammatory cytokines, chemokines, and hyaluronic acid using an enzyme-linked immunosorbent assay (ELISA) kit from R&D Systems, Minneapolis, MN, USA. Supplementary Table S2 provides information about the ELISA kits utilized in this study.

2.9. Real-time quantitative reverse transcription-polymerase chain reaction (qRT-PCR)

The HaCaT cells were seeded and cultured for 24 h. Following a change in the culture medium, the sample was added and incubated for an additional 24 h. To extract cellular mRNA, TRIzol lysis was performed after two washes with PBS from Invitrogen, Carlsbad, CA, USA. The RNA was then reverse transcribed into complementary DNA (cDNA) using an RNA-to-cDNA reverse transcription kit from Invitrogen, Carlsbad, CA, USA. Quantitative reverse transcription-polymerase chain reaction (qRT-PCR) was conducted using SYBR® Green Sensimix Plus Master Mix obtained from Quantace, Watford, UK. The primer sequences used in the experiment were provided by Macrogen, Seoul, Republic of Korea, and are listed in Supplementary Table S3. The threshold cycle of each reaction was determined, in our previous study (Wang et al., 2023). In this study, beta-actin served as the reference gene or housekeeping gene.

2.10. Western blotting

The HaCaT cells, after treatment, were lysed in RIPA lysis buffer obtained from Thermo Fisher Scientific, Waltham, MA, USA. A Thermo Fisher Scientific electrophoresis chamber was used to separate 50 µg of total protein using 10% sodium dodecyl sulfate–polyacrylamide gel electrophoresis (SDS-PAGE), and subsequently transferred to a polyvinylidene fluoride (PVDF) membrane. Prior to the addition of primary antibodies, the blots were blocked with 5% skim milk in phosphate-buffered saline (PBS) for 1 h at room temperature. The primary and secondary antibodies are listed in Supplementary Table S4. The membrane was incubated with a horseradish peroxidase (HRP)-conjugated secondary antibody for 1 h, followed by incubation with 0.1% Tris-buffered saline (TBS). Protein bands were detected and quantified using an enhanced chemiluminescence reagent from Thermo Fisher Scientific. Immunoreactive bands were visualized and quantified using the Alliance MINI HD9 AUTO Immunoblot Imaging System from UVItec Limited, England, UK, with the assistance of ImageJ software.

2.11. Statistical analysis

Three independent experiments were carried out in duplicate, and the results were expressed as the mean value along with the standard deviation (SD). Statistical analysis was performed using GraphPad Prism 8 software. Student's t-tests were employed to determine the statistical significance of observed differences. The significance thresholds for all comparisons were established as $*p < 0.05$, $**p < 0.01$, and $***p < 0.001$, respectively.

3. Results and discussion

3.1. Identification and quantification of flavonoids in IE extract using UPLC-MS/MS

To identify the primary phytochemicals in the IE extract, UPLC-MS/MS and MS were performed (Hwang et al., 2021). The photodiode array (PDA) chromatogram and base peak chromatogram (BPC) were analyzed, and the results are presented in Fig. S1 A–B. The mass-to-charge ratio (m/z) was determined using MS and tandem MS (MS/MS), and an in-house spectral library was used to identify the primary peaks with a mass accuracy of < 5 ppm. Three major peaks were identified in the BPC at retention periods of 6.48, 6.69, and 7.92 min, and their source ions at 611.1585, 465.1012, 294.1562, and 361.0901, respectively, were confirmed using MS analysis in positive ionized mode ([M + H] +). These peaks correspond to the three main flavonoids, rutin, hyperoside, and rosmarinic acid, in the IE extract. Therefore, these three flavonoids are regarded as major phytochemicals (Muvhulawa et al., 2022). Previously, Hong et al. identified five dimeric ent-kaurane diterpenoids isolated from the methanol extract of the aerial parts of IE. However, our research presents the initial evidence to demonstrate the presence of three established compounds, in IE: rutin, hyperoside, and rosmarinic acid.

3.2. Optimization of IE-AuNPs synthesis conditions

Plant leaf extracts contain a wide variety of bioactive phytomolecules such as alkaloids, flavonoids, tannins, phenolic compounds, saponins, and triterpenoids (Mlozi et al., 2022). Polyphenols and flavonoids present in the extract can convert gold ions to zero-valent molecules during the synthesis of compounds by reduction and oxidation reactions (Sabir, 2022). This process generates keto-form products and AuNPs, which are stabilized and encapsulated by the secondary metabolites present in the extract (Guan et al., 2022; M. Wang et al., 2021). Therefore, the leaf extract of this plant contains a variety of bioactive phytomolecules that can be used as reducing and capping agents in the synthesis of AuNPs. In our study, leaf tissue extract (IE) was used as a reducing and capping agent to synthesize IE-AuNPs. The synthesis process was personalized by adjusting various factors such as the concentration of gold salt and IE extract, as well as the temperature and duration of the reaction. The optimal values for the synthesis process were found to be 2.5 mg/mL for IE and 2 mM for $HAuCl_4\ 3H_2O$, with a temperature of 50 °C and a duration of 30 min (Fig. 1 A-D). The successful synthesis of IE-AuNPs was confirmed using UV–Vis spectra analysis and the purple color and the sharp peak at 548 nm corresponding to the localized surface plasmon resonance (LSPR) of the synthesized IE-AuNPs, as shown in Fig. 1 E. Optimum conditions are summarized in Fig. 1 F.

3.3. Physicochemical characterization of IE-AuNPs

Transmission electron microscopy (TEM) is a technique used to obtain high-quality images of nanoscale NPs. The size and shape of the synthesized NPs, as well as their reliable structural morphology, were observed in the TEM images (Ielo et al., 2021). Fig. 2 A depicts the shape of the synthesized AuNPs with sizes ranging 10–100 nm and shapes that are polygonal, triangular, and hexagonal, as determined by TEM images of the AuNPs. Furthermore, Fig. 2 B displays Energy-Dispersive X-ray Spectroscopy (EDS) mapping images of IE-AuNPs, wherein the localization of Au is emphasized by the color red. Based on the analysis of the EDX spectra, the optical absorption peaks corresponding to Au (2.1 keV) and copper (8 keV) were observed, respectively. Previous research suggested that the application of a copper grid for Transmission Electron Microscopy (TEM) structural evaluation may produce a copper peak (Ngo et al., 2022). XRD analysis is a technique used to determine the crystal structure and orientation of materials by analyzing the diffraction of X-rays by the crystal lattice planes (Bunaciu et al., 2015). In AuNPs, XRD analysis can reveal characteristic diffraction peaks that provide information about their crystal structure. In Fig. 2 C-D, XRD and SAED were employed to identify the crystal structure of IE-AuNPs. The observed primary peaks at 111, 200, 220, and 311 indicate a face-centered cubic crystal structure of the gold lattice planes of Bragg's reflection. The intensity of the (1 1 1) peak suggests a preferential orientation of the nanoparticles along this crystal plane. The (2 0 0), (2 2 0), and (3 1 1) peaks provide further insights into the arrangement of atoms within the nanoparticles (Dhandapani et al., 2021). The formation of a crystalline structure in AuNPs occurs during their synthesis process, as gold ions are reduced and stabilized, lead-

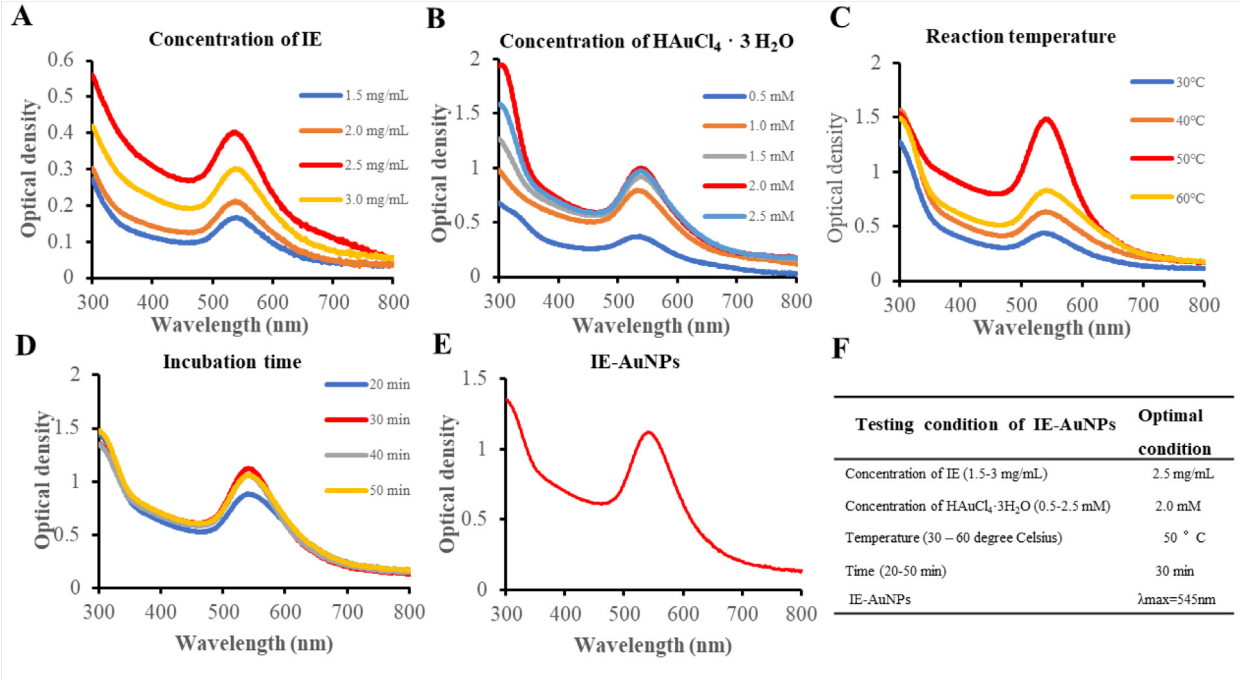

Fig. 1 The optimization of the synthesis of IE-AuNPs using UV–Vis spectroscopy. (A) IE concentrations ranging 1.5–3 mg/mL, (B) shows Au salt concentrations ranging 0.5–2.5 mM. (C) demonstrates the impact of temperature fluctuations (30–60 °C), and (D) represents the effect of the incubation period (20–50 min). The UV absorbance of the optimized IE-AuNPs at 545 nm is shown in (E), and (F) presents the optimal conditions for the synthesis of IE-AuNPs.

ing to the aggregation and arrangement of atoms into a regular crystal lattice (Kandathil & Manoj, 2023). In addition to XRD, SAED is another technique that can be used to study the crystal structure of AuNPs. By analyzing the diffraction patterns obtained from the interaction of a focused electron beam with the nanoparticles, can determine the crystal orientation and lattice arrangement, providing valuable information about the nanoparticle's crystalline nature and crystallographic properties (Bhamare, 2022; Rasmi & Mansoureh, 2022). Therefore, the XRD peaks and SAED observed in IE-AuNPs, including (111), (200), (220), and (311), indicate their crystalline structure and provide insights into their crystallographic orientation and arrangement. Moreover, as illustrated in Fig. S2, the TEM image analysis revealed an inter-planar distance (d) of 0.234 nm between parallel atomic planes. This distance corresponds to the (111) crystallographic plane, indicating a crystalline structure similar to the findings from XRD and SAED analyses. Upon performing the calculations, that the lattice parameter of the IE-AuNPs is a = 4.07. This lattice parameter corresponds to a specific inter-planar distance, providing valuable insights into the nanostructure and crystallographic arrangement of the synthesized nanoparticles. The consistency of these results further supports the presence of a well-defined crystalline structure in the synthesized nanoparticles. DLS analysis was conducted to determine the size characteristics of IE-AuNPs. In Fig. 2 E the results showed that the intensity size was measured at 135.40 nm, while the volume size was determined to be 127.00 nm. Although both TEM and DLS are used to measure particle size, the results may differ owing to their unique properties (Nojoki et al., 2022). Furthermore, AFM analysis was employed to validate the size of the IE-AuNPs, yielding measured size values of 98 nm (Fig. S3). The incorporation of AFM analysis allows for a more comprehensive understanding of the size and morphology of the IE-AuNPs in three dimensions. Multiple studies have documented that FT-IR analysis is advantageous for investigating the surface characteristics of plant-sourced AuNPs as well as for predicting potential interactions between the AuNPs and various functional groups. Therefore, the functional groups of IE-AuNPs, IE, and Au salts were analyzed using an FT-IR spectral library to confirm that IE was the basis for the synthesis of IE-AuNPs. In Fig. 2 F, the spectral analysis revealed distinctive bands observed at wavenumbers of 3340.7 cm^{-1} for the IE-AuNPs, 3310.0 cm^{-1} for IE, and 3331.15 cm^{-1} for the Au salt. These bands can be attributed to the O–H stretching group of phenols or alcohols, as indicated by the spectral library (Barabadi et al., 2015). The C–H stretch of the methylene groups of the protein was related to the bands at 2924.2 cm^{-1} of IE-AuNPs and 2926.8 of IE. The presence of the stretched C = O group can be identified by the band observed at a wavenumber of 1716.52 cm^{-1} for IE-AuNPs (R. Wang et al., 2021). The C = O stretching and C = C alkene bonding seemed to be attributed to the primary characteristic peaks at 1647.1 cm^{-1} for IE-AuNPs, 1691.5 cm^{-1} for IE and 1613.16 cm^{-1} for the Au salt, most likely due to the carbonyl group and amine (Das et al., 2011). The CH bending vibration results from the presence of alkenes and aliphatic amine functional groups, and it can be identified by the signals at 1366.2 cm^{-1} in IE-AuNPs and those at 1598.2 cm^{-1}, 1372.2 $cm^{-1}$and 1033.9 cm^{-1} in IE (Ahmad et al., 2017). Infrared (IR) spectra revealed that IE-AuNPs contain functional groups, including aromatic, hydroxyl, and carbonyl (aldehyde) groups, which are thought to originate from the flavonoids

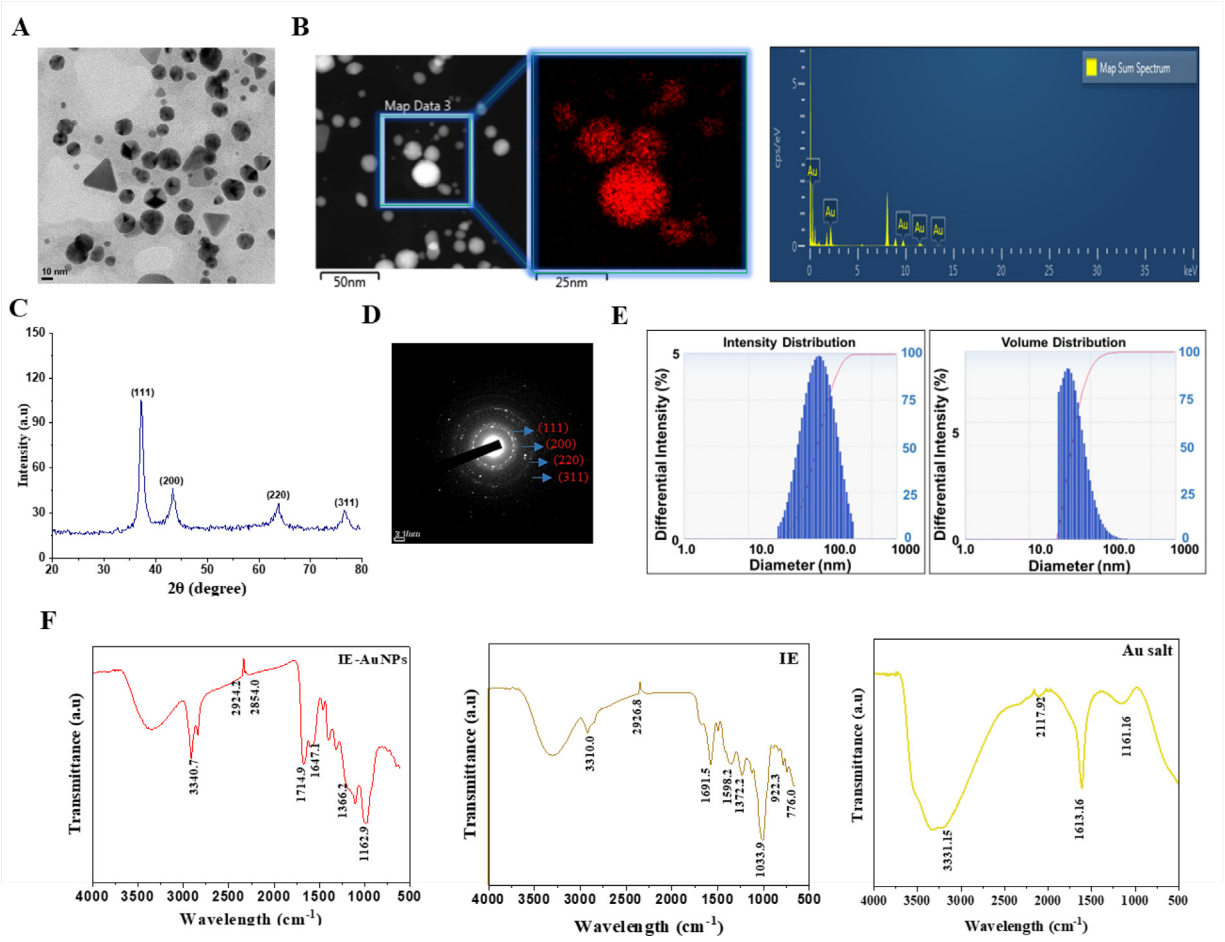

Fig. 2 Physiochemical characterization of IE-AuNPs. (A) Morphological properties of IE-AuNPs were determined using transmission electron microscopy (TEM). (B) Energy-dispersive X-ray (EDX) spectroscopy confirmed the elemental composition of IE-AuNPs. (C) X-ray diffraction (XRD) spectroscopy was used for crystalline structure determination of IE-AuNPs. (D) Crystalline structure of IE-AuNPs was determined using the selected area electron diffraction (SAED) pattern from TEM. (E) Dynamic light scattering (DLS) spectroscopy provided intensity and volume distributions of IE-AuNPs. (F) Infrared absorption spectrum produced using Fourier-transform infrared (FT-IR) spectroscopy for confirmation of chemical linkage confirmation in IE-AuNPs.

present in IE, such as rutin, hyperoside, and rosmarinic acid. Previous studies suggested that these flavonoids play crucial roles in the reduction, capping, and stabilization processes during the biosynthesis of AuNPs (Lee et al., 2020). Hence, it is plausible to propose that the hydroxyl and carbonyl groups, specifically those present in the mentioned flavonoids obtained from IE, function as active components responsible for the reduction, capping, and stabilization of the IE-AuNPs during the synthesis process. Finally, we conducted Zeta potential analysis of the IE-AuNPs both initially and after a six-month period to evaluate their long-term stability. As shown in Fig. S4 (A – B), the initial Zeta potential analysis revealed a value of −55.77 mV, indicating a highly stable dispersion with strong repulsion among the particles. This finding aligns with our previous characterization, highlighting the favorable stability of the IE-AuNPs under normal conditions. Following a six-month duration, the Zeta potential value showed a slight decrease to −44.67 mV. While this decrease suggests a reduction in stability compared to the initial measurement, it is important to note that the value remains relatively high. The Zeta potential value of −44.67 mV still signifies the presence of a significant repulsive force among the particles, contributing to their overall stability. In summary, the Zeta potential analysis confirms the favorable stability of the IE-AuNPs, as evidenced by the initial high Zeta potential value. Although a slight decrease in Zeta potential was observed after the six-month period, it is noteworthy that the value remains relatively high, indicating the presence of an appreciable repulsive force among the particles. This assessment of the Zeta potential provides valuable insights into the long-term stability of the IE-AuNPs and further supports their suitability for the intended application.

3.4. Evaluation of the cell viability and uptake of IE-AuNPs in HaCaT cells

The viability of HaCaT cells treated with IE-AuNPs and IE was evaluated using an MTT assay. Cells were treated with various concentrations of IE-AuNPs, dexamethasome (PC) and IE ranging 6.25–100 μg/mL, for 24 h. High doses (> 50 μg/mL) were found to be toxic, as shown in Fig. S5. Further studies were performed using non-toxic doses of IE-

AuNPs and IE with concentrations of 25 and 50 µg/mL and PC at 20 µg/mL (Fig. 3 A). Live/dead staining shown in Fig. 3 B, was performed to confirm the effects of IE-AuNPs and IE on HaCaT cells. No cytotoxicity was observed in HaCaT cells when IE was synthesized from IE-AuNPs.

The cellular uptake of IE-AuNPs into HaCaT cells was confirmed using EDF microscopy. In Fig. 3 C, DIC and TIRS images demonstrate that IE-AuNPs initially accumulated on the cell wall after 1 h and subsequently penetrated the cells after 3 h, indicating a time-dependent uptake.

Previous studies have demonstrated that NPs could be internalized into macrophages by fluid-phase endocytosis. The overall uptake of NPs was described as a two-step process, including the binding of NPs on the cell membrane and the internalization of the reactive sites by an endocytosis pathway (Olivieri et al., 2022). Similarly, we also observed that IE-AuNPs in HaCaT cells also displayed such two-step. That is, nanoparticle endocytosis is first triggered by an adsorption step on the outer membrane of the cell. A large number of studies have shown that the cell surface has many large anionic domains (Li et al., 2022). We therefore believe that the aggregation effect of anionic nanoparticles may be due to their repulsive interactions with negatively charged domains. The mechanism of nanoparticle penetration into keratinocytes gov-

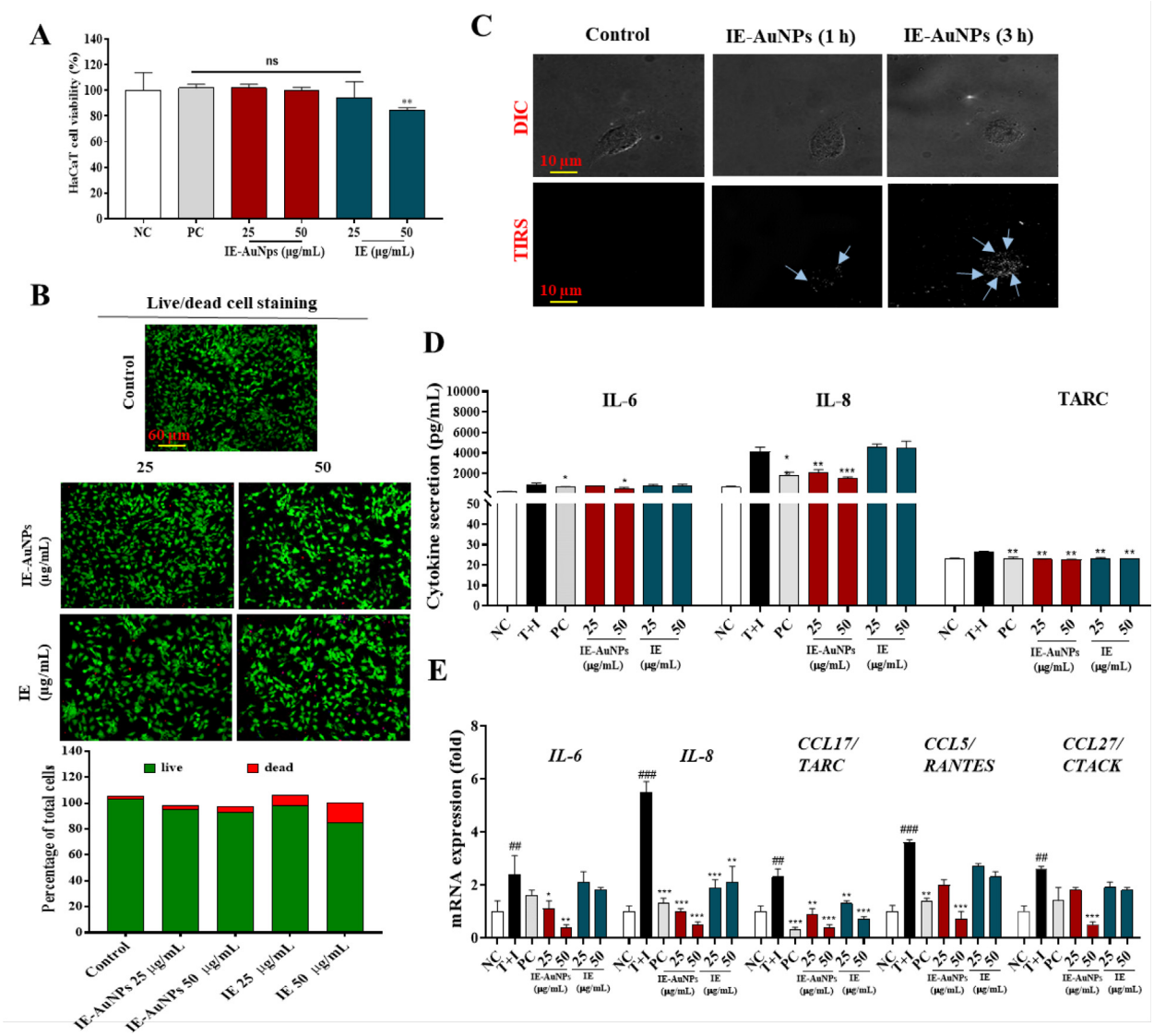

Fig. 3 Toxicity and anti-inflammatory activity evaluation of IE-AuNPs and IE against human epidermal keratinocytes (HaCaT cells). (A) Cell viability of IE-AuNPs, IE and PC on HaCaT cells, as determined using MTT assay. (B) LIVE and DEAD staining in IE-AuNPs and IE treated HaCaT cells. (C) Differential interference contrast (DIC) and total internal reflection scattering (TIRS) microscopic images of the cellular uptake of IE-AuNPs in HaCaT cells. (D) Cytokines secretion (IL-6, IL-8, and TARC) evaluation using ELISA. (E) The mRNA expression analysis of *IL-6*, *IL-8*, *CCL17*/*TARC*, *CCL5*/*RANTES*, and *CCL27*/*CTACK*. NC, negative control treated with medium alone; T + I, inflammation-induced control treated with T + I alone; PC, positive control treated with dexamethasone followed by T + I stimulation. The crosshatch marks indicate significant differences between NC and T + I, and asterisks indicate significant differences between T + I and each group. # and * $p < 0.05$; ## ** $p < 0.01$; and *** $p < 0.001$.

erned by diverse pathways and influenced by several nanoparticle characteristics (Augustine et al., 2020). Overall, our findings highlight the non-toxic nature of IE-AuNPs on HaCaT cells up to a concentration of 50 μg/mL and the temporal dynamics of their uptake.

3.5. Augmentation of anti-inflammatory activity in keratinocytes by treatment with IE-AuNPs

We explored the activty of IE-AuNPs on inflammatory skin diseases (ISDs) using HaCaT cells. Inflammatory skin conditions are caused by inflammatory chemokines and cytokines (Tsai et al., 2022). Epidermal keratinocytes, constituting approximately 90% of the cellular population within the epidermis, assume a pivotal role in the advancement and pathogenesis of dermatitis-associated disorders. They actively engage in intricate cellular interactions during inflammatory responses within the skin. The involvement of keratinocytes and their secreted CC chemokine ligands (CCLs), including CCL5 (RANTES), CCL17 (TARC), CCL22 (macrophage-derived chemokine, MDC), CCL27 (CTACK), as well as CXC chemokine ligands (CXCLs) such as CXCL8 (IL-8), has been well-established in the initiation and progression of inflammatory skin diseases. These chemokines function by orchestrating the recruitment of immune cells to the inflamed skin tissue. In particular, these inflammatory chemokines can be significantly upregulated in keratinocytes when stimulated with macrophages or T cell-secreting cytokines such as TNF-α and IFN-γ. Therefore, recent studies have focused on the potential of downregulating these inflammatory chemokines and understanding their underlying mechanisms of action in T + I-induced keratinocytes to develop effective treatments for ISDs. HaCaT cells stimulated with T + I (10 ng/mL) were treated with IE-AuNPs, IE, or PC. As shown in Fig. 3 D, the T + I-induced production of TARC/CCL17, interleukin 6 (IL-6), and interleukin 8 (IL-8) induced by T + I was inhibited by IE-AuNPs, IE, and PC. The mRNA expression levels of *IL-6*, *IL-8*, *TARC*/*CCL17*, normal T cell expressed and presumably secreted *(RANTES*/*CCL15*), and cutaneous T cell-attracting chemokine (*CTACK*/*CCL27*) were measured using qRT-PCR. Fig. 3 E shows that IE-AuNPs downregulated the expression of these genes in T + I-stimulated HaCaT cells, whereas IE and PC did not have as much of an effect. These findings indicate that IE-AuNPs can inhibit the expression of chemokines and cytokines induced by T + I in HaCaT cells, suggesting their ability as anti-inflammatory drugs for the treatment of ISDs.

3.6. Potential therapeutic application of IE-AuNPs for restoring mitochondrial function in inflammatory conditions of keratinocytes

Inflammation is a multifaceted biological reaction that tissues undergo in response to detrimental stimuli such as pathogens, injured cells, or irritants. Inflammatory reactions can lead to the generation of ROS and mito-SOX, which can damage cellular components and contribute to mitochondrial dysfunction. The involvement of impaired mitochondrial function has been implicated in the development of different inflammatory disorders, including diseases related to dermatitis. Recent studies have shown that NPs, such as AuNPs, can modulate cellular signaling and affect mitochondrial function. Therefore, we explored the activity of IE-AuNPs to prevent ROS and mito-SOX formation and to restore mitochondrial function in HaCaT cells treated with T + I, which mimics inflammatory conditions. In Fig. 4 A-B, results shows that IE-AuNPs had a higher ability to prevent ROS and Mito-SOX formation than IE, indicating their improved anti-inflammatory effects. Furthermore, as shown in Fig. 4 C-F, IE-AuNPs treatment resulted in increased expression of *TOM20* and *TIM23*, which are mitochondrial function markers, and decreased expression of *PINK1* and *PARKIN*, which was consistent with the results of western blotting (Fig. 4 G), suggesting that IE-AuNPs could restore the function of mitochondria damaged by T + I treatment. These findings suggested that IE-AuNPs have potential therapeutic applications in mitochondrial dysfunction-associated diseases, including inflammatory skin diseases.

3.7. IE-AuNPs modulate keratinocyte inflammatory response through autophagy-related signaling pathway

Inflammation is an intricate immune system response to detrimental stimuli, such as pathogens or damaged cells, characterized by complex biological processes. It regulated by various signaling pathways, and autophagy plays a main role in this process. Autophagy is a universally preserved cellular mechanism that encompasses the degradation of cellular constituents, including damaged organelles or protein aggregates, via the lysosomal machinery. The perturbation of autophagy has been implicated in numerous physiological processes, highlighting its significance in the exploration and development of novel therapeutic approaches for these diseases (Abad-Jiménez et al., 2022; Chen et al., 2022). Beclin1 plays a crucial role in initiating autophagosome formation and facilitates the recruitment of other autophagy-related genes (Atgs). The conversion of cytoplasmic LC3a to LC3b is a significant event in the activation of autophagy, and the LC3b/LC3a ratio serves as a widely employed indicator for monitoring autophagy. Additionally, p62 acts as a key mediator in identifying and transporting unwanted cargo to autophagosomes, ultimately leading to their degradation. Consequently, when autophagy flux is obstructed, the abundance of p62 protein increases, indicating its potential as a marker for autophagy impairment. Our results indicated that the increase in inflammasomes generated by T + I in HaCaT cells was significantly reduced by the addition of IE-AuNPs. Although T + I treatment decreased the expression of autophagy indicators, such as the conversion of *LC3-a* to *LC3-b* and the production of *Beclin1*, it increased the expression of *p62*, demonstrating the inhibition of autophagy in HaCaT Cells. In contrast,treatment with IE-AuNPs in HaCaT cells restored the autophagy markers to their prior levels of expression (Fig. 5 A–E), which shows that IE-AuNPs effectively promote the initiation and progression of the autophagic process.

Moreover, the autophagy signaling mechanism in the regulation of inflammation and autophagy in T + I induced HaCaT cells was investigated. Chloroquine (CQ), an inhibitor of autophagic flux that increases the LC3b/a ratio and p62 content, was used to block autophagy (Le et al., 2022;

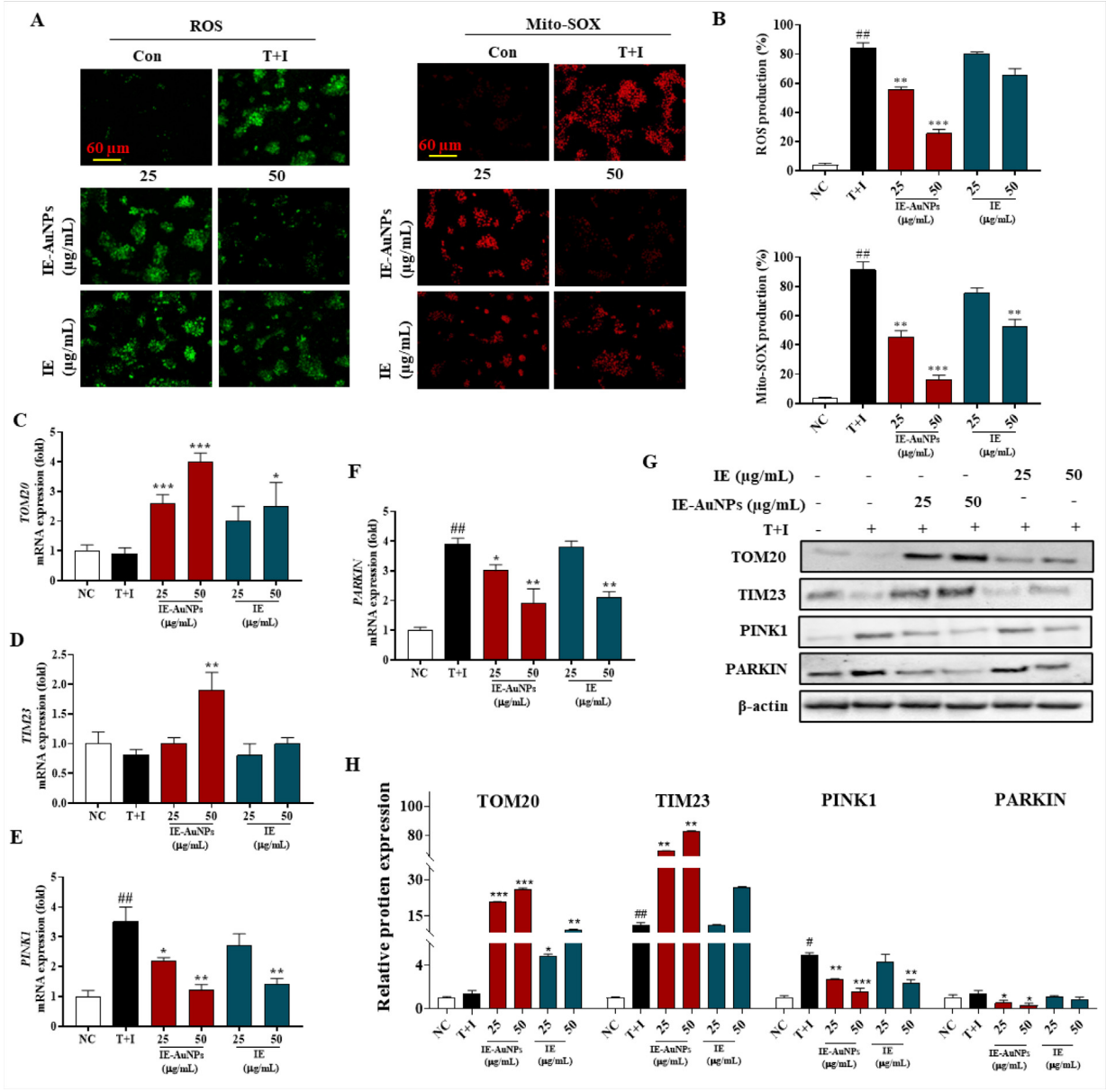

Fig. 4 IE-AuNPs alleviate T + I-induced mitochondrial dysfunction in HaCaT cells. (A) Fluorescence images and (B) quantification of the results from HaCaT cells treated with IE-AuNPs, following staining with ROS and Mito-SOX. (C) mRNA expression levels of *TOM20*, (D) *TIM23*, (E) *PINK1*, and (F) *PARKIN* were analyzed using qPCR. (G) Immunoblot analysis of TOM20, TIM23, PINK1, and PARKIN protein expression, with all bands standardized to β-actin. Negative control (NC) cells were treated with medium alone, inflammation-induced control (T + I) cells were treated with T + I alone. The crosshatch marks indicate significant differences between NC and T + I, and asterisks indicate significant differences between T + I and each group. # and * $p < 0.05$; ## *and* ** $p < 0.01$; and *** $p < 0.001$.

Stalnecker et al., 2022). Our results demonstrate that treatment with T + I resulted in a suppression of autophagy in HaCaT cells, whereas the treatment of IE-AuNPs significantly mitigated this effect (Fig. 5 F–G). Compared to cells that were not treated with CQ (50 μM), cells that had been co-treated with CQ and IE-AuNPs exhibited considerably induced expression of the mRNA and proteins of autophagy biomarkers. Additionally, CQ significantly increased the expression of p65, but the IE-AuNPs treatment group, which was made by T + I, was able to effectively turn this control around. p65 is an integral member of the nuclear factor kappa-light-chain-enhancer of activated B cells (NF-κB) transcription factor family, which consists of five components. As a component of the NF-κB signaling pathway, p65 plays a pivotal role in mediating the inflammatory response within the body. This pathway can be activated by various stressful stimuli, such as free radicals, tumor necrosis factor α (TNFα), interleukin 1-beta (IL-1β), or bacterial lipopolysaccharides (LPS). There-

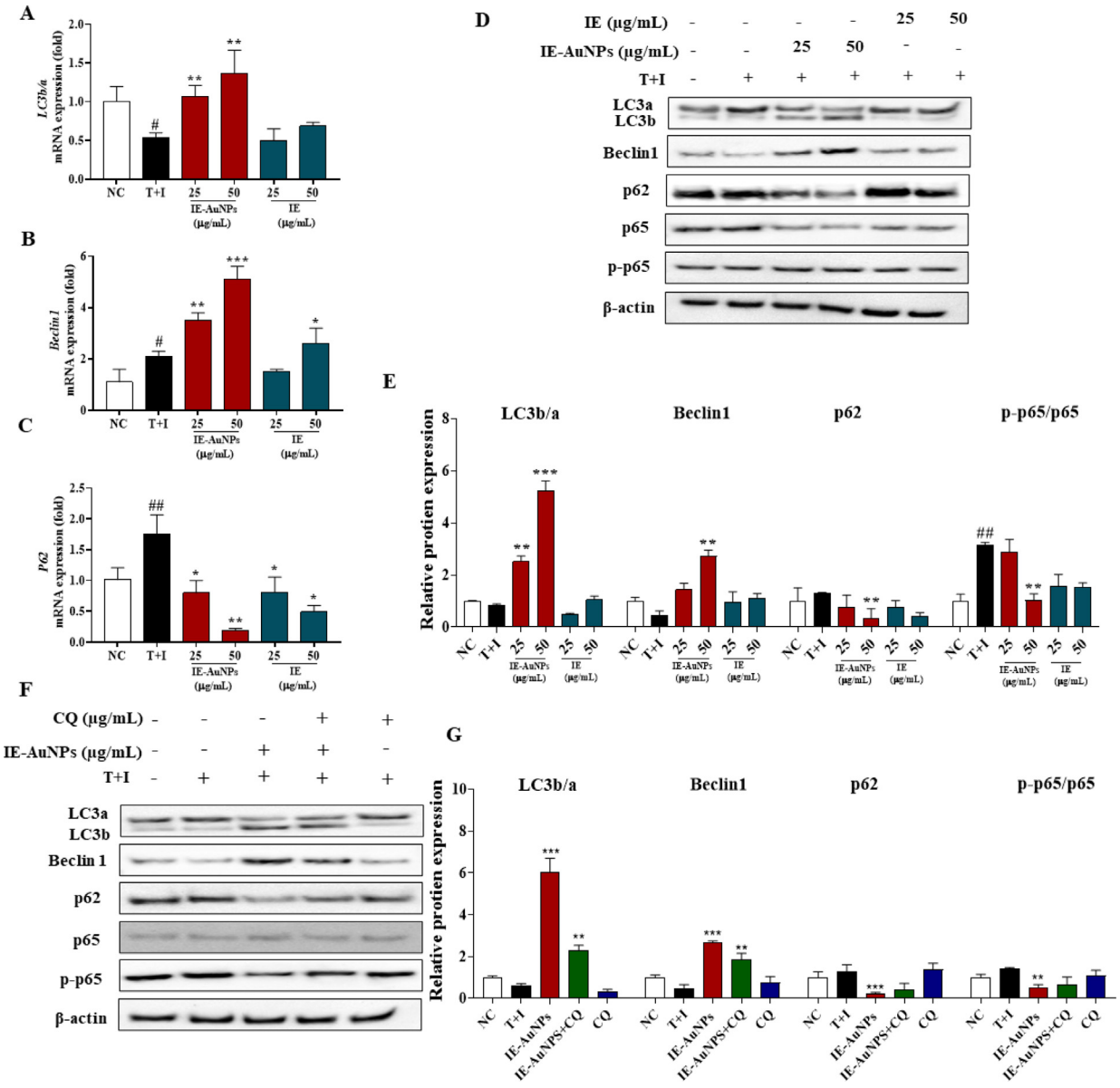

Fig. 5 IE-AuNPs enhance autophagic flux in HaCaT cells. (A) mRNA expression levels of *LC3b/a*, (B) *Beclin*, and (C) *p62* were analyzed using quantitative PCR. (D) Protein expression levels of LC3b/a, Beclin, p62, p65, and p-p65 were analyzed using immunoblotting. (E) Quantification of the results using Image J software. (F) Autophagy flux markers were inhibited by chloroquine (CQ). (G) Quantification of the results using Image J software. Negative control (NC) cells were treated with medium alone; inflammation-induced control (T + I) cells were treated with T + I alone. The crosshatch marks indicate significant differences between NC and T + I, and asterisks indicate significant differences between T + I and each group. # and * $p < 0.05$; ## *and* ** $p < 0.01$; and *** $p < 0.001$.

fore, we suggest that IE-AuNPs can modulate the inflammatory signaling pathway through an autophagy-related signaling pathway, as indicated by all these studies when considered simultaneously.

3.8. IE-AuNPs down-regulate PI3K/AKT/mTOR signaling pathway to activate autophagy and reduce keratinocyte inflammatory response

The PI3K/Akt/mTOR pathway is a well-established signaling pathway involved in the initiation of autophagy. There is substantial evidence suggesting that compounds that enhance autophagy by inhibiting this signalling pathway can reduce endothelial cell apoptosis induced by the combination of T + I. It is necessary for both the inflammatory response and autophagy (J. Wang et al., 2022; Xiao et al., 2022). Here, we further investigated whether IE-AuNPs had any influence on the this signaling pathway to exhibit anti-inflammatory activity. In contrast to the group that had been treated only with T + I, the expression levels of PI3K, AKT, and their downstream protein p70SK6 were lower in the groups that had been treated with IE-AuNPs and IE, as shown by the

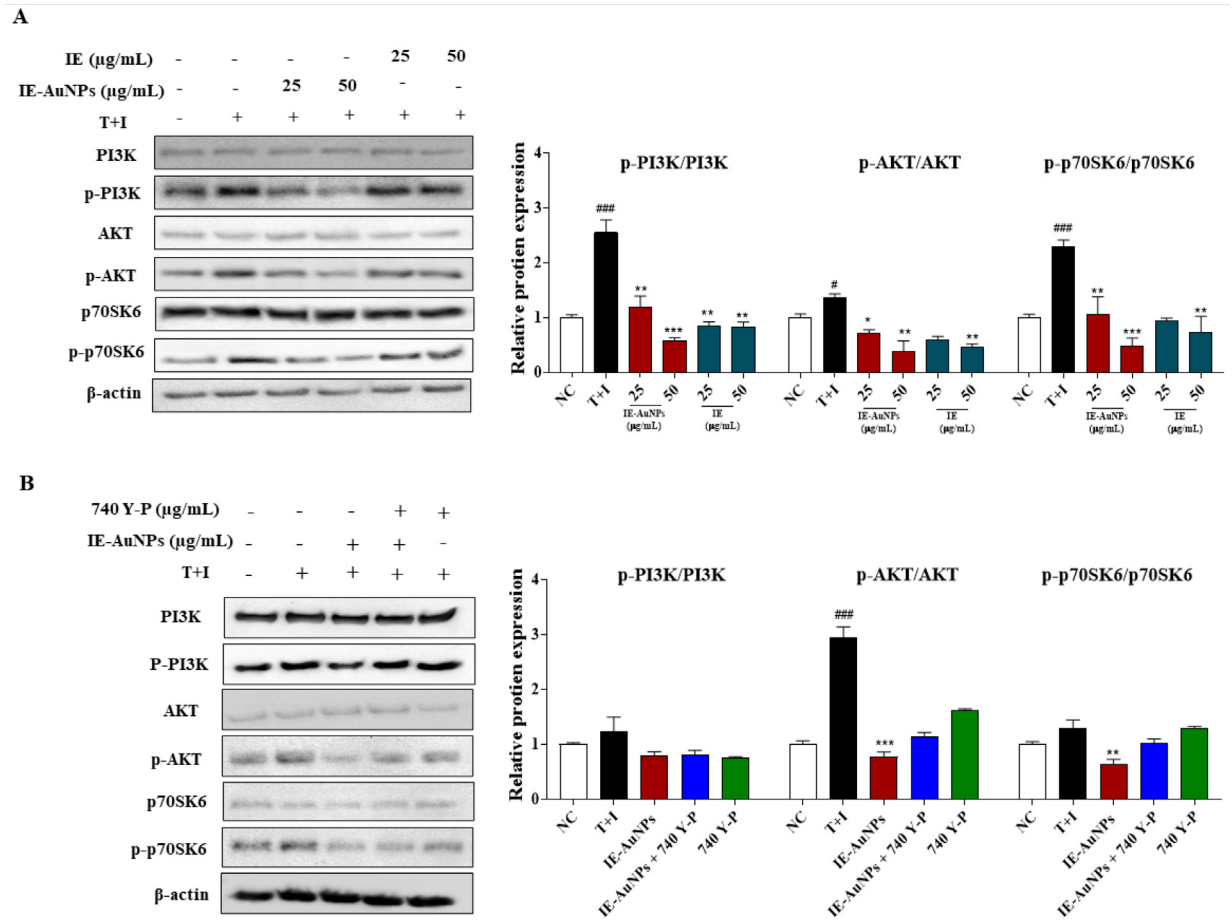

Fig. 6 The mechanism of IE-AuNPs in suppressing pro-inflammatory mediators and inducing autophagy through the PI3K/AKT signaling pathway. (A) shows the protein expression of PI3K, p-PI3K, AKT, p-AKT, p70SK6, and p-p70SK6 analyzed using immunoblotting, and all their bands were analyzed and standardized to β-actin. (B) shows the effect of IE-AuNPs on the PI3K/AKT signaling pathway in HaCaT cells with the application of the PI3K activator 740Y-P (30 μM). The negative control (NC) was treated with medium alone, and the inflammation-induced control (T + I) was treated with T + I alone. The crosshatch marks indicate significant differences between NC and T + I, and asterisks indicate significant differences between T + I and each group. # and * $p < 0.05$; ## *and* ** $p < 0.01$; and *** $p < 0.001$.

western blot analysis in Fig. 6 A-B. These results suggest that IE-AuNPs supressed the PI3K/Akt/mTOR cascade, we demonstrated whether IE-AuNPs enhanced autophagy by activation of the PI3K/Akt/mTOR pathway. In Fig. 6 B, we observed that the activity of IE-AuNPs upregulated the LC3b/a ratio and suppressed the p62 levels in keratinocytes and this effect were reversed by treatment with the PI3K agonist 740 Y-P. This demonstrated that the PI3K/AKT/mTORC1 pathway induced by T + I was downregulated by IE and IE-AuNPs, which may play a role in activating autophagy in cells. Similar to our results, Wang et al. reported that biologically synthesized black ginger-selenium NPs induced autophagy in AGS cells by inhibiting the PI3K/Akt/mTOR signaling pathway (R. Wang et al., 2022). Therefore, we conclude that IE-AuNPs successfully inhibit T + I-induced keratinocyte inflammatory response. It is probable that enhancing the rate of autophagic flux progression is the key to achieving these effects.

4. Conclusion

In this study, IE-AuNPs were synthesized and characterized and their potential for treating inflammatory skin disorders was investigated. TEM and EDX imaging confirmed that the synthesized IE-AuNPs were polygonal, triangular, and hexagonal in shape, and were primarily composed of Au. XRD and SAED analyses revealed that the IE-AuNPs were crystalline. IE-AuNPs did not cause cytotoxicity in HaCaT cells and exhibited a reliable duration of cell penetration after 3 h. Furthermore, IE-AuNPs inhibited the formation of ROS, MitoSOX, and mitochondrial dysfunction indicators, such as PINK1 and PARKIN, in HaCaT cells. Treatment with IE-AuNPs resulted in the suppression of anti-inflammatory cytokines and chemokines expression, along with the activation of autophagy biomarkers. These effects were observed through the downregulation of the PI3K/AKT/mTORC1 signaling pathway. The promising therapeutic potential of IE-AuNPs for the prevention and treatment of various skin-related disorders is highlighted by these results. However, further research is needed to explore the interactions between different cell types and structures within the complex organ of the skin, which consists of multiple layers and distinct cell types. Additionally, there is a need to

investigate the potential therapeutic applications of IE-AuNPs in diverse skin conditions. By pursuing these future research directions, the field can continue to advance and innovative strategies for managing skin inflammation and developing dermatological therapeutics can be developed.

CRediT authorship contribution statement

Sanjeevram Dhandapani: Formal analysis, Data curation, Writing – original draft. **Rongbo Wang:** Methodology, Data curation. **Ki cheol Hwang:** Conceptualization, Resources. **Hoon Kim:** Methodology. **Yeon-Ju Kim:** Project administration, Supervision.

Declaration of Competing Interest

The authors declare that they have no known competing financial interests or personal relationships that could have appeared to influence the work reported in this paper.

Acknowledgement

This work was carried out with the support of "Cooperative Research Program for Agriculture Science and Technology Development (PJ01703502)" Rural Development Administration, Republic of Korea.

Appendix A. Supplementary material

Supplementary data to this article can be found online at https://doi.org/10.1016/j.arabjc.2023.105113.

References

Abad-Jiménez, Z., López-Domènech, S., García-Gargallo, C., Vezza, T., Gómez-Abril, S.Á., Morillas, C., Díaz-Pozo, P., Falcón, R., Bañuls, C., Víctor, V.M., 2022. Roux-en-Y gastric bypass modulates AMPK, autophagy and inflammatory response in leukocytes of obese patients. Biomedicines 10 (2), 430.

Abdel-Mageed, H.M., AbuelEzz, N.Z., Radwan, R.A., Mohamed, S. A., 2021. Nanoparticles in nanomedicine: a comprehensive updated review on current status, challenges and emerging opportunities. J. Microencapsul. 38 (6), 414–436.

Ahmad, N., Bhatnagar, S., Saxena, R., Iqbal, D., Ghosh, A.K., Dutta, R., 2017. Biosynthesis and characterization of gold nanoparticles: Kinetics, in vitro and in vivo study. Mater. Sci. Eng. C 78, 553–564.

Anik, M.I., Mahmud, N., Al Masud, A., Hasan, M., 2022. Gold nanoparticles (GNPs) in biomedical and clinical applications: A review. Nano Select 3 (4), 792–828.

Barabadi, H., Honary, S., Ebrahimi, P., Mohammadi, M.A., Alizadeh, A., Naghibi, F., 2015. Microbial mediated preparation, characterization and optimization of gold nanoparticles. Braz. J. Microbiol. 45 (4), 1493–1501.

Bhamare, V.S., 2022. Mechanistic insight into photocatalytic degradation of antibiotic cefadroxil by 5% barium/zinc oxide nanocomposite during water treatment. Emerg. Mater. 5 (2), 413–429.

Bunaciu, A.A., UdriŞTioiu, E.G., Aboul-Enein, H.Y., 2015. X-ray diffraction: instrumentation and applications. Crit. Rev. Anal. Chem. 45 (4), 289–299.

Calabrese, L., Fiocco, Z., Satoh, T.K., Peris, K., French, L.E., 2022. Therapeutic potential of targeting interleukin-1 family cytokines in chronic inflammatory skin diseases. Br. J. Dermatol. 186 (6), 925–941.

Chen, Y., Lei, L., Wang, K., Liang, R., Qiao, Y., Feng, Z., Zhang, J., Bai, M., Chen, H., Zhao, J., 2022. Huangqi-Honghua combination prevents cerebral infarction with Qi deficiency and blood stasis syndrome in rats by the autophagy pathway. Evid. Based Complement. Alternat. Med. 2022, 9496926.

Das, R.K., Gogoi, N., Bora, U., 2011. Green synthesis of gold nanoparticles using Nyctanthes arbortristis flower extract. Bioprocess Biosyst. Eng. 34 (5), 615–619.

Dhandapani, S., Wang, R., cheol Hwang, K., Kim, H., & Kim, Y.J. (2023). Enhanced skin anti-inflammatory and moisturizing action of gold nanoparticles produced utilizing Diospyros kaki fruit extracts. *Arabian Journal of Chemistry*, *16*(4), 104551.

Dhandapani, S., Xu, X., Wang, R., Puja, A.M., Kim, H., Perumalsamy, H., Balusamy, S.R., Kim, Y.-J., 2021. Biosynthesis of gold nanoparticles using Nigella sativa and Curtobacterium proimmune K3 and evaluation of their anticancer activity. Mater. Sci. Eng. C 127, 112214.

Firdhouse, M.J., Lalitha, P., 2022. Biogenic green synthesis of gold nanoparticles and their applications–A review of promising properties. Inorg. Chem. Commun. 143, 109800.

Guan, J., Wu, C., He, Y., Lu, F., 2023. Skin-associated adipocytes in skin barrier immunity: A mini-review. Front. Immunol. 14, 1116548.

Guan, Z., Ying, S., Ofoegbu, P.C., Clubb, P., Rico, C., He, F., Hong, J., 2022. Green synthesis of nanoparticles: Current developments and limitations. Environ. Technol. Innov. 26, 102336.

Hosny, M., Fawzy, M., El-Badry, Y.A., Hussein, E.E., Eltaweil, A.S., 2022. Plant-assisted synthesis of gold nanoparticles for photocatalytic, anticancer, and antioxidant applications. J. Saudi Chem. Soc. 26, (2) 101419.

Hwang, K.C., Shin, H.Y., Kim, W.J., Seo, M.S., Kim, H., 2021. Effects of a high-molecular-weight polysaccharides isolated from Korean persimmon on the antioxidant, anti-inflammatory, and antiwrinkle activity. Molecules 26 (6), 1600.

Ielo, I., Rando, G., Giacobello, F., Sfameni, S., Castellano, A., Galletta, M., Drommi, D., Rosace, G., Plutino, M.R., 2021. Synthesis, chemical–physical characterization, and biomedical applications of functional gold nanoparticles: A review. Molecules 26 (19), 5823.

Irfan, M., Moniruzzaman, M., Ahmad, T., Samsudin, M.F.R., Bashir, F., Butt, M.T., Ashraf, H., 2022. Identifying the role of process conditions for synthesis of stable gold nanoparticles and insight detail of reaction mechanism. Inorg. Nano-Metal Chem. 52 (4), 519–532.

Kandathil, V., Manoj, N., 2023. Advances in CO2 utilization employing anisotropic nanomaterials as catalysts: a review. Front. Chem. 11, 1175132.

Kashaf, S. S., Harkins, C. P., Deming, C., Joglekar, P., Conlan, S., Holmes, C. J., Almeida, A., Finn, R. D., Segre, J. A., & Kong, H. H. (2023). Staphylococcal diversity in atopic dermatitis from an individual to a global scale. *Cell host & microbe*, *31*(4), 578-592. e576.

Kerketta, A., & Sahu, B. (2023). Nanomaterials synthesis from medicinal plant extract. *Phytochemicals in Medicinal Plants: Biodiversity, Bioactivity and Drug Discovery*, *291*.

Khan, F., Shariq, M., Asif, M., Siddiqui, M.A., Malan, P., Ahmad, F., 2022. Green nanotechnology: plant-mediated nanoparticle synthesis and application. Nanomaterials 12 (4), 673.

Kumar, R., Ranjith, S., Balu, H., Bharathi, D., Chandan, K., Ahmed, S.S., 2022. Role of nanotechnology in biomedical applications: an updated review. UPI J. Pharma. Med. Health Sci. 5 (39), 43.

Le, T.V., Dinh, N.B.T., Dang, M.T., Phan, N.C.L., Dang, L.T.T., Grassi, G., Holterman, A.X.L., Le, H.M., Truong, N.H., 2022. Effects of autophagy inhibition by chloroquine on hepatic stellate cell activation in CCl4-induced acute liver injury mouse model. J. Gastroenterol. Hepatol. 37 (1), 216–224.

Lee, K.X., Shameli, K., Yew, Y.P., Teow, S.-Y., Jahangirian, H., Rafiee-Moghaddam, R., Webster, T.J., 2020. Recent developments

in the facile bio-synthesis of gold nanoparticles (AuNPs) and their biomedical applications. Int. J. Nanomed. 15, 275–300.
Li, X., Zhou, S., Lin, X., 2022. Molecular view on the impact of dha molecules on the physical properties of a model cell membrane. J. Chem. Inf. Model. 62 (10), 2421–2431.
Mlozi, S.H., Mmongoyo, J.A., Chacha, M., 2022. GC-MS analysis of bioactive phytochemicals from methanolic leaf and root extracts of Tephrosia vogelii. Scient. Afr. 16, e01255.
Muvhulawa, N., Dludla, P.V., Ziqubu, K., Mthembu, S.X., Mthiyane, F., Nkambule, B.B., Mazibuko-Mbeje, S.E., 2022. Rutin ameliorates inflammation and improves metabolic function: A comprehensive analysis of scientific literature. Pharmacol. Res. 178, 106163.
Nadaf, S.J., Jadhav, N.R., Naikwadi, H.S., Savekar, P.L., Sapkal, I. D., Kambli, M.M., Desai, I.A., 2022. Green synthesis of gold and silver nanoparticles: Updates on research, patents, and future prospects. OpenNano 8, 100076.
Ngo, N.M., Omidiyan, M., Tran, H.-V., Lee, T.R., 2022. Stable semi-hollow gold-silver nanostars with tunable plasmonic resonances ranging from ultraviolet-visible to near-infrared wavelengths: Implications for photocatalysis, biosensing, and theranostics. ACS Appl. Nano Mater. 8, 11391.
Nojoki, F., Ebrahimi-Hosseinzadeh, B., Hatamian-Zarmi, A., Khodagholi, F., Khezri, K., 2022. Design and development of chitosan-insulin-transfersomes (Transfersulin) as effective intranasal nanovesicles for the treatment of Alzheimer's disease: In vitro, in vivo, and ex vivo evaluations. Biomed. Pharmacother. 153, 113450.
Olivieri, P.H., Jesus, M.B., Nader, H.B., Justo, G.Z., Sousa, A.A., 2022. Cell-surface glycosaminoglycans regulate the cellular uptake of charged polystyrene nanoparticles. Nanoscale 14 (19), 7350–7363.
Papa, V., Li Pomi, F., Borgia, F., Vaccaro, M., Pioggia, G., Gangemi, S., 2023. Immunosenescence and skin: A state of art of its etiopathogenetic role and crucial watershed for systemic implications. Int. J. Mol. Sci. 24 (9), 7956.
Rani, N., Singh, P., Kumar, S., Kumar, P., Bhankar, V., Kumar, K., 2023. Plant-mediated synthesis of nanoparticles and their applications: A review. Mater. Res. Bull. 163, 112233.
Rasmi, Y., & Mansoureh, N. V. (2022). Characterization of nanoparticles: methods and techniques. In *Applications of Nanotechnology in Drug Discovery and Delivery*, 95-116.
Roy, A., Pandit, C., Gacem, A., Alqahtani, M.S., Bilal, M., Islam, S., Hossain, M.J., Jameel, M., 2022. Biologically derived gold nanoparticles and their applications. Bioinorg. Chem. Appl. 2022, 8184217.
Sabir, F. (2022). Biotechnological Approaches for the Production of Immunomodulating Phytomolecules. In *Plants and Phytomolecules for Immunomodulation*, 493-518.
Sahu, A., Singh, P., Singh, P., Singh Gahlot, A.P., Mehrotra, R., 2022. Simple and rapid biogenic synthesis of colloidal silver and gold nanoparticles using Aegle marmelos fruit for SERS detection of DNA. Inorg. Nano-Metal Chem. 1, 12.
Shahin, T.B., Sreekantaswamy, S.A., Hawkes, J.E., Butler, D.C., 2023. Treatment strategies for chronic pruritus and eczema/dermatitis in older adults under the category of chronic eczematous eruptions of aging (CEEA). Am. J. Clin. Dermatol. 24 (3), 405–418.
Sobhy, Y., Mady, M., Mina, S., Abo-zeid, Y., 2022. Phytochemical and pharmacological values of two major constituents of asparagus species and their nano formulations: A review. J. Adv. Pharm. Res. 6 (3), 94–106.
Stalnecker, C.A., Grover, K.R., Edwards, A.C., Coleman, M.F., Yang, R., DeLiberty, J.M., Papke, B., Goodwin, C.M., Pierobon, M., Petricoin, E.F., 2022. Concurrent inhibition of IGF1R and ERK increases pancreatic cancer sensitivity to autophagy InhibitorsIGF1R inhibition enhances dual ERK and autophagy inhibition. Cancer Res. 82 (4), 586–598.
Tai, Y., Sakaida, Y., Kawasaki, R., Kanemaru, K., Akimoto, K., Brombacher, F., Ogawa, S., Nakamura, Y., Harada, Y., 2023. Foxp3 and Bcl6 deficiency synergistically induces spontaneous development of atopic dermatitis-like skin disease. Int. Immunol. 10, 1093.
Tsai, Y.-C., Chang, H.-H., Chou, S.-C., Chu, T.W., Hsu, Y.-J., Hsiao, C.-Y., Lo, Y.-H., Wu, N.-L., Chang, D.-C., Hung, C.-F., 2022. Evaluation of the anti-atopic dermatitis effects of α-boswellic acid on Tnf-α/Ifn-γ-stimulated HaCat cells and DNCB-induced BALB/c mice. Int. J. Mol. Sci. 23 (17), 9863.
Wang, J., Gao, X., Liu, F., Dong, J., Zhao, P., 2022. Difenoconazole causes cardiotoxicity in common carp (Cyprinus carpio): Involvement of oxidative stress, inflammation, apoptosis and autophagy. Chemosphere 306, 135562.
Wang, R., Ha, K.-Y., Dhandapani, S., Kim, Y.-J., 2022. Biologically synthesized black ginger-selenium nanoparticle induces apoptosis and autophagy of AGS gastric cancer cells by suppressing the PI3K/Akt/mTOR signaling pathway. J. Nanobiotechnol. 20 (1), 1–20.
Wang, R., Lee, Y.-G., Dhandapani, S., Baek, N.-I., Kim, K.-P., Cho, Y.-E., Xu, X., Kim, Y.-J., 2023. 8-paradol from ginger exacerbates PINK1/Parkin mediated mitophagy to induce apoptosis in human gastric adenocarcinoma. Pharmacol. Res. 187, 106610.
Wang, M., Meng, Y., Zhu, H., Hu, Y., Xu, C.-P., Chao, X., Li, W., Li, C., Pan, C., 2021. Green synthesized gold nanoparticles using Viola betonicifolia leaves extract: Characterization, antimicrobial, antioxidant, and cytobiocompatible activities. Int. J. Nanomed. 16, 7319.
Wang, R., Xu, X., Puja, A.M., Perumalsamy, H., Balusamy, S.R., Kim, H., Kim, Y.J., 2021. Gold nanoparticles prepared with Phyllanthus emblica fruit extract and Bifidobacterium animalis subsp. lactis can induce apoptosis via mitochondrial impairment with inhibition of autophagy in the human gastric carcinoma cell line AGS. Nanomaterials 11 (5).
Xiao, Q., Zhao, Z., Teng, Y., Wu, L., Wang, J., Xu, H., Chen, S., Zhou, Q., 2022. BMSC-derived exosomes alleviate intervertebral disc degeneration by modulating AKT/mTOR-mediated autophagy of nucleus pulposus cells. Stem Cells Int. 2022, 9896444.